Comparing myocardial shear wave propagation velocity estimation methods based on tissue displacement, velocity and acceleration data

Seliverstova E.[1], Caenen A.[1,2], Bézy S.[1], Nooijens S.[1], Voigt JU.[1], D'hooge J.[1]

[1]KU Leuven, Leuven, Belgium
[2]Ghent University, Ghent, Belgium

Address for Correspondence:
Ekaterina Seliverstova,
3000 Leuven, Belgium
UZ Herestraat 49 – box 7003
E-mail: ekaterina.seliverstova@kuleuven.be
Phone: (498) 496-927

Abstract: Shear wave elastography (SWE) is a promising technique to non-invasively assess cardiac function through the evaluation of cardiac stiffness. However, in the literature, SWE varies in terms of analysed tissue motion data (displacement, velocity or acceleration); method to characterize mechanical wave propagation (time domain (TD) vs. frequency domain (FD)); and the metric reported (wave speed (WS), shear or Young's modulus). This variety of reported methodologies complicates comparison of reported findings and sheds doubt on which methodology better approximates the true myocardial properties. We, therefore, conducted a simulation study to investigate the accuracy of various SWE data analysis approaches while varying cardiac geometry and stiffness. Lower WS values were obtained by the TD method compared to the FD method. Acceleration-based WS estimates in the TD were systematically larger than those based on velocity (~10% difference). These observations were confirmed by TD analysis of 32 *in vivo* SWE mechanical wave measurements. *In vivo* data quality is typically too low for accurate FD analysis. Therefore, our study suggests using acceleration based TD analysis for *in vivo* SWE to minimize the underestimation of the true WS and thus to maximize the sensitivity of SWE to detect stiffness changes due to pathology.

Keywords: cardiac imaging; shear wave elastography; ultrasound Tissue Doppler imaging; Fourier analysis

Introduction

Cardiac dysfunction is a frequent and significant problem in our society as it is associated with high mortality and morbidity rates (Savarese and Lund 2017). Therefore, the field of cardiac diagnostics is exploring methods to improve cardiac function assessment by potentially including measurements of mechanical tissue properties next to conventionally measured metrics of cardiac morphology, tissue and blood flow velocities (Nagueh et al. 2016). Indeed, information on mechanical tissue properties can help to monitor and treat cardiac diseases (Golob et al. 2014) in the same way as it has proven successful in diagnosing breast tumours and staging liver fibrosis (Guerra et al. 2015; Jayaraman et al. 2017). Furthermore, tissue elasticity enables to relate measured myocardial deformation from strain imaging to the acting forces within the myocardial wall and can therefore improve our understanding of cardiac function (Elgeti et al. 2014; Voigt 2019).

Ultrasound shear wave elastography (SWE) provides a non-invasive way to measure myocardial stiffness and it comprises three stages. The first stage is tissue excitation, in which a mechanical wave can be excited naturally by a physiological event such as valve closure, or externally with acoustic radiation force (ARF). Shear waves are defined by a particle displacement perpendicular to the wave's travelling direction. The induced tissue motion after excitation is then estimated in the second stage of SWE using high frame rate ultrasound imaging (>500 Hz). At last, the third stage is a calculation of the measured tissue motion and the wave propagation velocity. In case of an isotropic homogeneous incompressible linear elastic unbounded medium, the shear stiffness μ or the Young's modulus $\mathbf{E}$ is directly related to the shear wave propagation velocity C_T :

$$\mu = \frac{1}{3}E = \rho C_T^2, \quad (1)$$

with ρ the medium's density.

A variety of analysis methods has been reported in literature for the third stage of cardiac SWE, as is summarized in Table (Appendix A). Note that this table does not give a complete overview of all cardiac SWE studies performed in literature. The wave propagation analysis varies in terms of (i) analysed type of particle motion data, (ii) the wave propagation characterization method and (iii) the reported metric. We will shortly describe each of these factors separately. First, three different types of particle motion data have been reported for SWE analysis: tissue displacement, velocity or acceleration (Bouchard et al. 2011; Kvåle et al. 2020; Rouze et al. 2018; Salles et al. 2021). However, as wave dispersion might occur because of the viscoelasticity and geometry of the myocardium, the wave propagation speeds estimated based on displacement, velocity or acceleration do not correspond necessarily. Rouze et al. (Rouze et al. 2018) even used the difference in wave propagation speeds derived from these signals to predict tissue viscoelasticity for bulk viscoelastic media. Second, many wave propagation characterization methods have been proposed (Kijanka and Urban 2021; Pernot et al. 2010; Rouze et al. 2018; Strachinaru et al. 2017a; Trutna et al. 2020) for estimating myocardial material properties, and they can be categorized into two classes: time domain (TD) and frequency domain (FD) methods. TD methods typically measure the mechanical wave propagation speed by tracking the wave's position in the spatiotemporal domain. The analysis of the wave propagation in the FD requires a Fourier transform, resulting in the frequency dependent phase speed, which can be transformed into a group speed or intrinsic material characteristics by fitting a model (Bernal et al. 2011). In literature (Bernal et al. 2011; Kanai 2005), the use of the zero-order asymmetric mode of the Lamb wave

model, describing wave propagation in a fluid-loaded elastic plate, has been reported to approach the mechanical wave travelling along the cardiac wall. The phase velocity curve of the A0-mode increases as a function of frequency until it reaches a plateau-value approaching the bulk SWS (Rose 2014). This model explains the expected differences in wave propagation speed estimated from different types of particle motion data: analysing acceleration data will yield wave speed estimates closest to the bulk SWS due to its higher frequency content. Third, wave speed, shear modulus or Young's modulus has been reported as metric in cardiac SWE, depending on the used wave propagation characterization method (TD/FD) and the assumed material model. It is important to note that applying equation (1) to reconstruct the elastic modulus from the group velocity comes with the assumption of isotropy, homogeneity, incompressibility, linear elasticity and bulkiness none of which holds for the myocardium (Pelivanov et al. 2019).

It should be noted that the studied wave in SWE is not by definition a shear wave due to the heart's geometry and complex material properties. Therefore, we refer to the studied wave with more general terms such as 'wave' and 'mechanical wave' throughout the manuscript, but the technology itself is still referred to as shear wave elastography (SWE) as that naming has historically grown.

Different SWE analysis approaches resulted in a wide range of reported propagation speed or tissue stiffness as shown in Table (Appendix A). It is however unclear how each method performs on the same dataset, and how the reported metric relates to the true material's stiffness in cardiac SWE. Furthermore, these results might be highly dependent on the considered cardiac geometry and (visco)elastic material properties, as velocity dispersion can be present. Therefore, the objective of this work was to systematically investigate the accuracy of often-recurring settings in cardiac SWE data analysis for various cardiac geometries and material properties. In particular, we studied the effect of considering different quantities describing tissue motion (displacement/velocity/acceleration) and the effect of applying time vs. FD approaches on the accuracy of mechanical wave speed estimation.

Materials and Methods

Virtual wave propagation datasets mimicking natural cardiac SWE were generated using the open-source k-Wave V1.3 toolbox (Treeby and Cox 2010) in MATLAB R2018a (MathWorks, Natick, MA, USA). More specifically, the pstdElastic2D script simulates waves in a viscoelastic medium relying on the Kelvin-Voigt material model. The left ventricle (LV) of the heart was approximated as a 2D truncated ellipsoid (Bankman 2009), of which the LV cavity was 41.8 mm along the major axis and 25 mm along the minor axis (see). We considered 9 different LV sizes with the thickness along the minor axis a varying from 4.2 to 10.5 mm and the thickness along the major axis b changing from 6 to 15 mm Fig.1, covering a wide range of values typically reported in the clinic for healthy volunteers (±2 standard deviations) (Kou et al. 2014) and for patients with cardiac amyloidosis (Petrescu et al. 2019). A LV shear stiffness between 1 to 108 kPa and a shear viscosity between 6.3 to 6300 mPa·s was considered to mimic clinical relevant values (Kanai 2009). Both material parameters are directly depending on the bulk shear wave speed (SWS) in the k-Wave simulation toolbox, which was varied from 1 to 10 m/s in steps of 1 m/s to obtain the before mentioned ranges of shear stiffness and viscosity. The mechanical wave excitation source was located at the base of the LV (see Fig.1). Mitral valve closure (MVC) was modelled by imposing a transversal velocity (25 mm/s) as a band

filtered single sine cycle at 50 Hz (Arnott et al. 1984; Finel 2018; Vos et al. 2017), as visualized at the inlet of the LV in Fig.1.

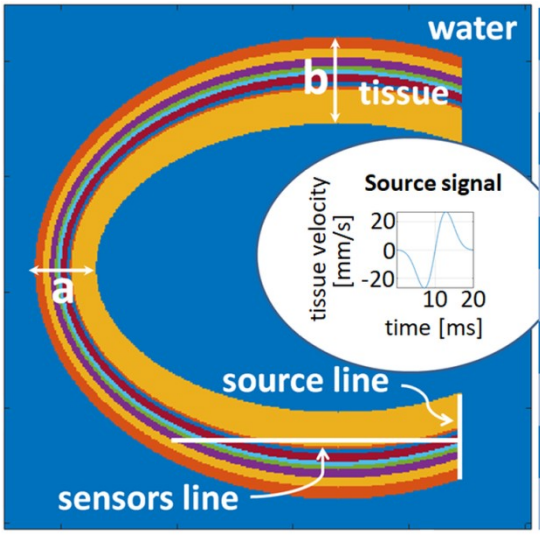

b [mm]	a [mm]
6	4.2
6.5	4.5
7.2	5
8.6	6
9.3	6.6
10	7
11.4	8
13	9.1
15	10.5

Fig.1. Simulation geometry. The ellipsoidal shape represents the heart model, in which the different colours visualize the 9 different LV sizes that were considered: the dimensions of the LV cavity did not change, but the cardiac wall thickness altered according to the thickness variations as tabulated in the table on the right, with 'a' the thickness along the ellipse major axis and 'b' the thickness along the ellipse minor axis. The blue region represents the surrounding tissues modelled as water. The white vertical line of single pixels at the bottom right is a wave source that mimics valve closure (i.e. band filtered single sine cycle at 50 Hz); whereas the horizontal white line at the bottom is a single pixel line that consists of sensors recording data during the simulation (M-mode line). The position of this sensor line shifts in the vertical direction to be located at the middle of the cardiac wall depending on the chosen wall thickness. The M-line has a length of 35 mm for all simulations.

A summary of the general parameters used for the simulation setup is presented in Table 1. A grid optimization study in terms of computational time and accuracy was performed to select the optimal full field size (91x91 mm) and grid spacing (0.25x0.25 mm). A perfectly matched layer (PML) of 20 grid points was modelled at the edges of the grid to absorb any oscillations and avoid reflections. The time step in the k-Wave simulation was automatically determined from the Courant-Friedrichs-Lewy number (CFL), prescribing the ratio of the distance a wave can travel in one time step and the grid spacing. After optimization, a CFL value of 0.1 was chosen for better accuracy while still fulfilling the k-Wave recommendation of CFL≤0.3. A total of 90 simulations (9 geometries and 10 bulk shear wave propagation velocity values) were run on a Vlaams Supercomputer Center (VSC)-cluster with 2 Xeon Gold 6140 CPUs@2.3 GHz and 18 cores (each 192 GB RAM).

Tissue motion data was collected along a straight line of sensors on the cardiac wall (see Fig.1) to create an M-mode image (as done in clinical studies, e.g. (Petrescu et al. 2020). These sensors recorded tissue velocities at every time instance of the simulation. The data was down sampled to a resolution of 16 µs afterwards. To approximate a typical parasternal long axis Doppler recording, only the components of the recorded velocities that are normal to the sensor line were considered. To get displacement and acceleration M-modes, the velocity data

was integrated and temporally derivated respectively. An example of the resulting M-mode images in displacement, velocity and acceleration is shown in Fig.2.

Table 1 – Parameters used for simulations.

Thickness along major ellipse axis a [mm]	4.2-10.5
Thickness along minor ellipse axis b [mm]	6-15
Nx/Ny (full simulation field size)	364/364
PML size (at the edges additional to Nx/Ny)	20
Grid step size dx/dy [mm] (same for all simulations)	0.25/0.25
CFL (same for all simulations)	0.1
dt [ns] (same for all simulations)	16
Downsampling after simulation dt [µs]	16
Compressional speed [m/s] (tissue and blood)	1540
Transversal speed [m/s]	1-10
Blood density (close to water density) [kg/m^3]	1050
tissue density [kg/m^3]	1081
absorption coefficient for compression waves [dB/(MHz^2 cm)]	1
absorption coefficient for shear waves [dB/(MHz^2 cm)]	10^7

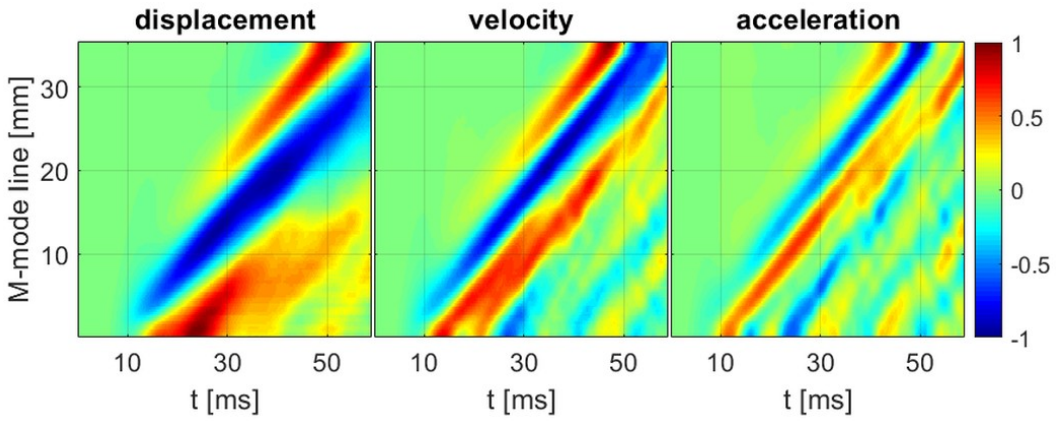

Fig.2. Illustrative simulated M-mode image showing the individually normalized tissue displacement, velocity and acceleration of a model with b=6 mm and bulk shear wave speed (SWS) = 1 m/s.

We considered two methods to estimate the WS from the tissue motion data, one in the TD and one in the FD. The selected TD method is a typical time of flight method that characterizes mechanical wave position as a function of time. In particular, the slope detection method (Santos et al. 2019) of the in-house developed SPEQLE software was used on the M-mode recording, and this software has yet been used in various clinical studies (Cvijic et al. 2020; Petrescu et al. 2019). The method consists of three steps: (i) smoothing the M-mode image with a kernel of 11 elements in space (~2.2 mm) and 139 elements in time (~2.3 ms) (ii) tracking a wave over time using the cross-correlation method and (iii) fitting a line and obtaining WS via the slope.

For the FD method, the region of interest in the M-mode was first zero-padded to obtain a matrix size that is a power of two in each dimension to optimize computation time. The edges of the space-time acceleration data were further interpolated using a sigmoid function (size adapted according to the region of interest) to reduce windowing-related artefacts, and subsequently the 2D Fast Fourier transform was applied. The result is represented in the wavenumber-frequency (k-f) FD. The group velocity $\boldsymbol{V_g}$ is defined as:

$$V_g \equiv \frac{d\omega}{dk}, (2)$$

with ω the angular frequency and k the spatial frequency. Detecting the slope of the wave mode with the maximum intensity on the k-f image then gives the group velocity:

$$\mathrm{V_g} = \frac{1}{\tan(\alpha)}, \qquad (3)$$

with α the slope of the inclination angle. Therefore, the wave mode with maximum energy was tracked by obtaining the wave number with maximum energy for every frequency. The tracked points with a magnitude in Fourier energy larger than -12 dB of the maximum energy were then considered in a least-squares fit to determine α and consecutively V_g (Nightingale et al. 2015).

For each simulation, the group velocity was estimated with the TD M-mode slope detection and the FD k-f image slope detection. This was done for displacement, velocity and acceleration data, resulting in 6 different WS estimates for all 90 simulated cases.

To support and verify the findings from the simulations, the SWE data of 32 *in vivo* measurements were considered (for this retrospective study all in vivo measurements were taken from KU Leuven database; human participants gave informed consent prior to enrollment; the original studies were approved by the local ethical committee with following numbers: S60439, S62685, P041/2019; more detailed information on the population is described in Appendix B). The SPEQLE software used in *in vivo* clinical studies at our lab only allowed for analysis of velocities and accelerations, thus only velocities and accelerations were examined in the TD and FD. As most of the data sets were not normally distributed (according to the Shapiro-Wilk test), WS results of the different methodologies applied to simulated and clinical data were compared using a Wilcoxon signed-rank test. A p-value smaller than 0.05/9≈0.006 was considered statistically significant for simulation data after applying Bonferroni Correction for repeated comparisons.

Results

Fig.3 shows representative M-mode images in tissue velocity together with the estimated WS in the TD, and Fig.4 represents the same cases in the FD with their WS estimates. As expected, both figures show that the detected WS increased with stiffness (i.e. the bulk SWS definition in k-Wave) and wall thickness (i.e. *b*), corresponding to what could be expected from the Lamb wave theory when assuming a zero-order antisymmetric (A0) mode excitation because of the direction of the imposed load. For ellipsoidal LV model, the estimated group WS was higher with the k-f image slope detection method than with the M-mode slope detection method (e.g. a LV with a base thickness of 6 mm and a bulk SWS of 3 m/s yields 1.4 m/s in the TD and 2.8 m/s in the FD). The top right panel of Fig.4 (b=15 mm and bulk SWS 1 m/s) illustrates two slopes, corresponding to the A0 and S0 mode. Only the WS value of the A0-mode was considered for further analysis. It can also be noted that a rippling effect appears in

the Fourier energies when bulk SWS increased (see Fig.4), due to a decreased time interval for the signal to be observed (similar to a windowing effect).

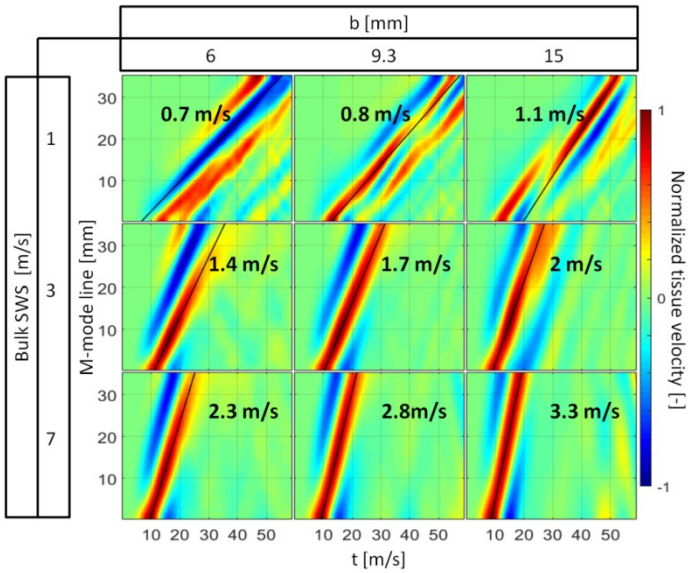

Fig.3. Simulated M-mode images (normalized tissue velocity data) for bulk SWS (shear wave speed) values of 1, 3 and 7 m/s and b (wall thickness) values of 6, 9.3 and 15 mm. The slope of the black line depicts the measured WS.

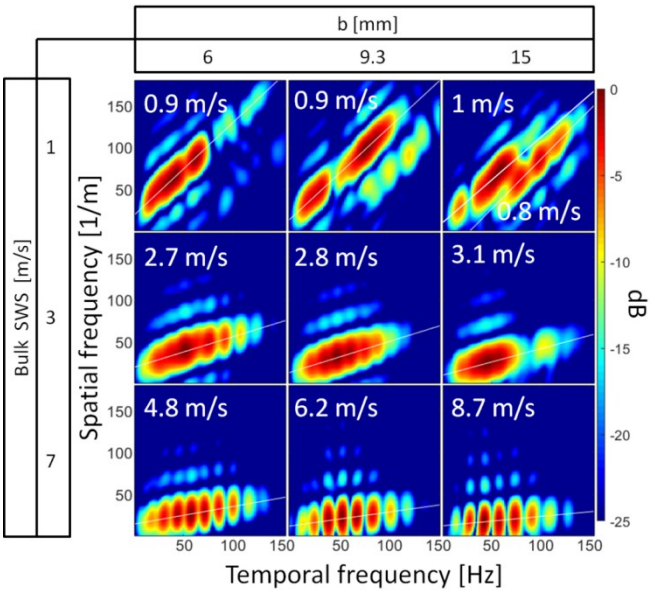

Fig.4. Frequency domain (FD) k-f images obtained from tissue velocity data, for bulk SWS (shear wave speed) values of 1, 3 and 7 m/s and b (wall thickness) values of 6, 9.3 and 15 mm. The white slope depicts the measured WS. The two slopes present at the top right image for b=15 mm and bulk SWS 1 m/s correspond to the A0 and S0 mode respectively.

The WS results from all simulations are summarized in Fig.5. There is a clear difference between WS values measured in the FD and the TD with those measured in the FD being markedly larger, regardless of the type of tissue motion considered. For example, for a LV thickness of 9.3 mm and a bulk speed of 3 m/s, the WS derived with the FD method is 67% larger than the one estimated with the TD method, when considering tissue acceleration data.

Furthermore, in the TD, there was a clear difference for displacement, velocity and acceleration data with WS estimates based on displacements being the lowest and those based on acceleration the highest (e.g. WS of 1.5 m/s, 1.7 m/s and 1.8 m/s for displacement, velocity and acceleration respectively in a LV model with a base thickness of 9.3 mm and a bulk SWS of 3 m/s).

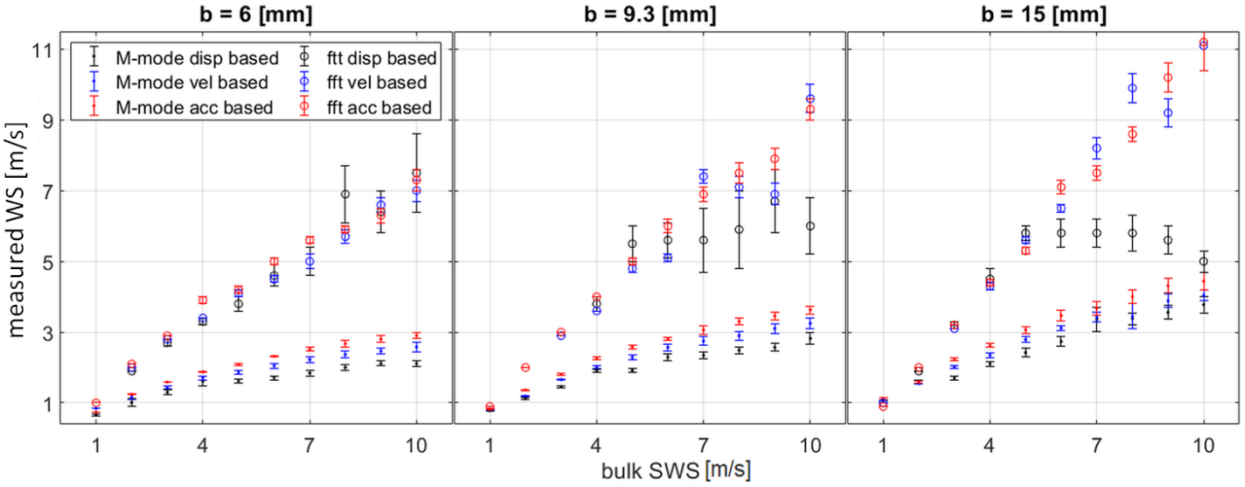

Fig.5. The estimated WS values for the three wall thickness values (*b*) and ten bulk SWS simulation setups. Error bars represent the standard deviation of 5 measurements in case of the time domain (TD) methodology and the standard deviation of the linear fit in case of the FD method.

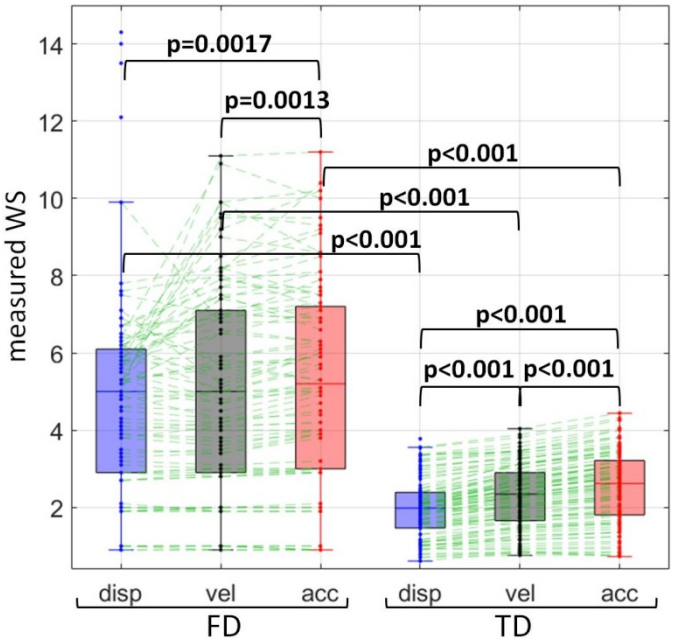

Fig.6. WS estimates made by 6 approaches on all 90 simulated data sets. All methods within TD and FD were compared to each other and also the methods within TD and FD for one specific tissue motion signal. A statistical significance level of 0.05/9 ≈ 0.006 was considered after taking Bonferroni correction into account.

The above-mentioned trends for the three geometries are statistically significant as demonstrated in Fig.6. The values extracted in the FD did not show a significant difference between displacement and velocity data (p=0.97) and displacement and acceleration data (p=0.65); whereas a significant difference was found between

velocity and acceleration data (p=0.004). On the other hand, significant differences were observed for all estimation methods in the TD with acceleration-based values being significantly higher and displacement-based values being significantly lower.

For the clinical data, WS estimation in the FD showed poor performance (only 12 out of 32 could reliably be estimated) compared to the TD methods (25 out of 32). Therefore, only the TD results are depicted in Fig.7.c showing a significant difference (p = 0.004) between WS measured on the velocity and acceleration data respectively. The mean of the relative difference between the propagation speeds estimated from tissue velocities and accelerations was 10%, which is similar to the results obtained from our simulations (9%).

Discussion

In cardiac SWE, various approaches have been reported to characterise mechanical wave propagation using tissue displacement, velocity or acceleration data in the time or frequency domain. However, as wave velocity dispersion might be present during wave propagation, these six approaches do not necessarily result in the same outcome. Therefore, we considered a simulation framework that provides access to the ground truth tissue characteristics, to investigate the effect of geometry and material properties on the accuracy of these six commonly used methodologies within cardiac SWE in a systematic way. The results showed that WS evaluation in the TD yielded in general lower WS estimates than the Fourier-based analysis (see Fig.6) – especially for increased wall thickness and stiffness as present in cardiac disease (for example hypertrophic cardiomyopathy) –, and showed significant differences in WS estimates in the TD for a different types of tissue motion (max. difference of 35% and 18% for displacement and velocity respectively compared to acceleration).

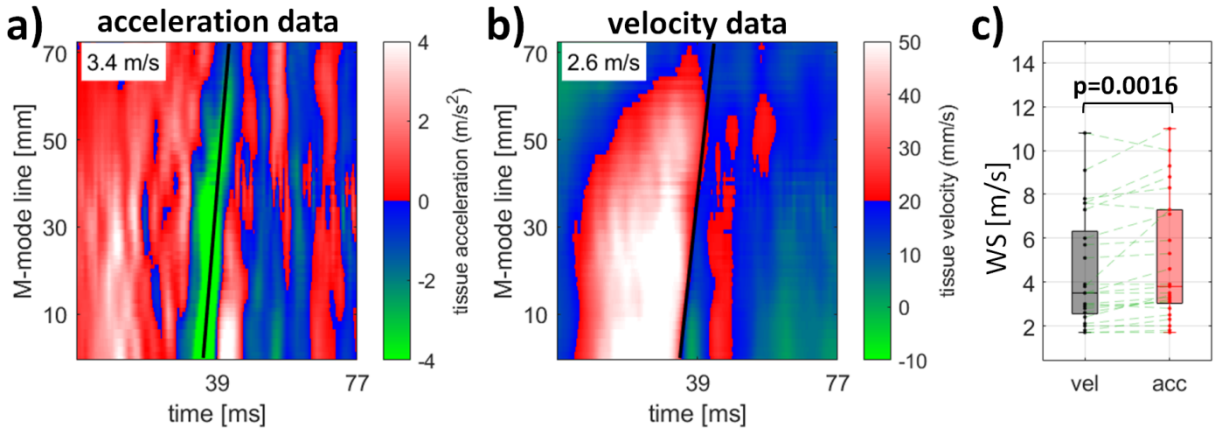

Fig.7. in vivo data: a) example of an individual WS slope estimation based on acceleration data; b) example of an individual WS slope estimation based on velocity data; c) the resulting WS values distribution made in 25 measurements (statistically significant p< 0.05).

This study is the first to systematically compare the results of time and frequency domain approaches for various clinical relevant cardiac geometries and material properties, according to the best of the authors' knowledge. Some cardiac ARF-based SWE studies (Nenadic et al. 2018; Pislaru et al. 2014) involving *in vivo* animals did describe the results of both the time and FD methods but these studies implemented the FD method differently: instead of determining a group speed as described in equations (2) and (3), these studies assumed a Lamb wave propagation

with a specific rheological model after Fourier analysis to determine elasticity (and viscosity). The advantage of our approach is that no model concerning mechanical wave or material properties needs to be assumed. However, we assumed the group velocity to be linearly dependent on the frequency in equation (3), whereas in general this dependency is nonlinear. Despite this limitation, the linear model fit well for the particular cases described in this paper (maximum relative standard error of the estimated slopes was 17%). It should also be noted that the FD approach becomes inadequate for tissue displacement data at high SW velocities for the larger thicknesses (bulk SWS>6 m/s at b=15 mm). This is probably due to the smaller number of data points available for fitting the k-f slope compared to velocity or acceleration data. This is especially true for natural waves, of which the frequency content is typically low (<150 Hz). Therefore, displacement-based frequency domain analysis is not reliable. In general, all six WS estimation approaches seemed to underestimate the actual stiffness – represented by the bulk SWS in k-Wave – for all considered geometries and material properties (see Fig.5). However, the bulk SWS cannot be treated as the reference speed by which the wave effectively travels in the considered LV model as it is affected by velocity dispersion due to the cardiac morphology and viscoelastic material properties. The Fourier method is therefore the benchmark method that determines the true SW speed, but the numerical accuracy of current simulation set-up of a LV model is unknown. Therefore, to validate our simulation set-up we also simulated SW propagation in a plate model with a thickness 8.5 mm and a bulk SWS of 3 m/s, where a theoretical solution is at hand. Figure 8a and b illustrate the results in the FD of the simulated plate in comparison with the A0-mode of the analytical Lamb wave model: the simulated dispersion curve fits the analytical Lamb dispersion curve well and the k-f image slope detection method yields a wave speed of 2.7 m/s (underestimation of 10% compared to bulk SWS) for both simulation and theory. The good correspondence between simulation and theory demonstrates the reliability of the numerical settings of our simulations, confirming that the outcome of the FD method applied to the simulations is accurate enough to be used as benchmark. It should however be noted that a few simulations yielded a WS estimate in the FD larger than the bulk SWS (especially in LV models with large thickness and high stiffness, see Fig.5 and Fig.6), whereas this should be in theory lower than the plate velocity (95% of the bulk SWS). This can be explained by the (k,f)-grid dependency of the accuracy of the WS estimation in the Fourier domain: the higher the WS detected, the lower the slope and the more sensitive the slope estimation is to the (k,f)-grid size. The accuracy can be improved by refining the spatial and/or temporal resolution of the simulations or zero padding the fast Fourier transform, but this requires more memory and calculation time.

The TD method dramatically underestimated the true WS obtained with the FD method for natural mechanical waves in the heart (see Fig.6). As demonstrated in Fig.8.c, the speed that we are measuring in the TD rather corresponded to the phase velocity at the centre frequency of the pulse rather than the true group speed derived from the Fourier analysis, mainly explaining the observed underestimation. An underestimation of the WS in the TD method was also previously reported for ARF-induced waves in LV phantom experiments and simulations (Caenen et al. 2017a) and arterial phantom experiments (Maksuti et al. 2016). Note however that the frequency content of ARF-induced cardiac mechanical waves are in general higher than that of natural mechanical waves (up to 500 Hz vs. 150 Hz (Kanai 2005; Sarvazyan et al. 2013; Vos et al. 2017)).

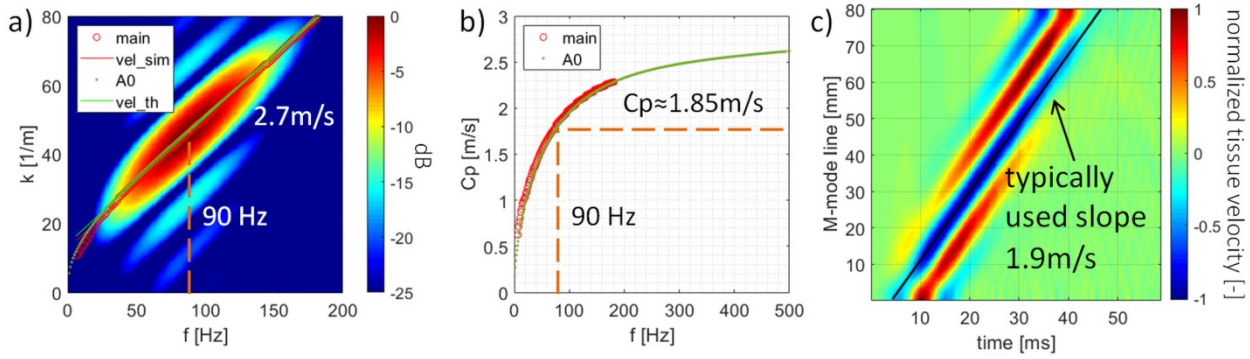

Fig.8. WS estimation in the TD and FD using acceleration data in a simulated plate with a thickness of 8.5 mm and a bulk SWS of 3 m/s in comparison to the zero-order antisymmetric mode (A0) of the Lamb wave theory. FD images in wavenumber-frequency (k-f; panel a) and phase velocity-frequency (cp-f; panel b) show the dispersion curve extracted from the simulation data (red circles) in combination with the dispersion curve calculated from the Lamb wave model (green dots). Red and green lines in panel a yield the velocity estimate (2.7 and 2.7 m/s) with the k-f slope detection method for the same frequency range for simulation and theory respectively, demonstrating a solid match. The simulated acceleration data of the M-mode is depicted in panel c, illustrating the WS estimate in the TD (1.9 m/s). The WS estimate in the TD corresponds to the phase speed of 1.85 m/s at the centre frequency of the shear wave (90 Hz).

The use of different types of tissue motion signals (displacement, velocity and acceleration) in the WS analysis showed statistical differences between the WS estimates in the TD and in the FD (only between velocity and acceleration), as illustrated in Fig.6. Also, there was a clear trend noticeable: WS estimates from tissue acceleration data were higher than that from tissue velocity data, which was again higher than that from tissue displacement data (median values of 1.98 m/s, 2.34 m/s and 2.62 m/s for displacement, velocity and acceleration in Fig.6). This trend is expected as phase speed is expected to increase with frequency (as stated by the A0 Lamb wave model (Rose 2014)), and taking the derivative in the TD means multiplying with frequency in the FD, which indicates that the larger phase velocities at higher frequency are weighted more heavily for the acceleration data compared to the velocity and displacement data. These observations are in line with previous work in three *in vivo* pigs (Keijzer et al. 2018) demonstrating a higher propagation speed for acceleration than velocity panels for 12 SWE measurements after aortic valve closure (median speed of 5.8 m/s vs. 5.1 m/s). Additionally, similar trends were found by Rouze et al. (Rouze et al. 2018) in bulky viscoelastic phantoms, in which phase speed also increased as a function of frequency, even though the origin of dispersion was solely due to viscoelasticity. Furthermore, the difference between WS estimates based on different types of motion signals in the TD got larger when bulk SWS and thickness increased (see Fig.5). WS estimation based on tissue acceleration yields thus the smallest underestimation of the true speed. Furthermore, it gives the largest sensitivity (detection range of 0.9-3.8 m/s, 0.9-4 m/s and 0.9-4.4 m/s for displacement, velocity and acceleration for all considered material properties in Fig.5).

Frequency analysis is the preferred way of characterizing wave propagation in cardiac SWE from a theoretical point of view, but its clinical applicability is still questionable as the Fourier domain of *in vivo* cardiac SWE data has typically a poor resolution (conventionally a time resolution of min. 0.75 ms within an observed time window of 40 ms and a space resolution of minimal 0.3 mm within a field of view of 30-120 mm for a parasternal

long axis view of the interventricular septum, it should however be noted that in vivo SWE data are typically up-sampled with a factor 10-50 in time to increase the time resolution of the wave speed estimator, resulting in a similar time resolution for simulations and experiments). The feasibility of the FD analysis might be improved by using an S-transform instead of FFT, as recently shown in application to liver (Kijanka and Urban 2021), but this should be investigated for cardiac SWE. Most research on cardiac SWE has thus far focused on the TD methods for wave characterization. These considerations are in line with our observations of the human SWE data: WS estimation in the FD was successful in only 12 out of 32 cases, whereas TD analysis showed a better feasibility (25 out of 32). Due to the low success rate of the FD method, this method was refrained from further comparison. A Wilcoxon signed-rank test for WS estimates based on velocity and acceleration data in the TD demonstrated a significant difference ($p = 0.004$), with a relative difference in WS of 10%. This is in line with the observed difference in the simulation data (9%). This difference in propagation speed should be taken into account when comparing various clinical studies and when setting cut-off values for diagnosis.

Even though our simulations provided the advantage of access to the full control of the true tissue mechanical properties, there are some limitations inherently linked to the simulation framework. First, the myocardium was modelled as a linear viscoelastic isotropic media, whereas it is generally known that material nonlinearity and anisotropy can also affect wave propagation (Bezy et al. 2021; Caenen et al. 2017b; Couade et al. 2011; E.M.Lifshitz 1970). Second, even though the theoretical validation of the plate model in Fig.8 showed the accuracy of our selected numerical settings, a true experimental validation of wave propagation in a LV model is missing.

Conclusions

This work numerically studied the accuracy of cardiac SWE analysis methods to characterize wave propagation in the TD and FD by using tissue displacement, velocity and acceleration for various cardiac morphologies and material properties. Ideally, FD methods are used for wave propagation characterization, but this can be challenging *in vivo* because of the limited temporal and spatial resolution and image quality. Significantly lower propagation speeds were obtained for the TD methods compared to the true wave speed as obtained by the FD method, especially for thick and stiff myocardium (as in cardiac disease). WS underestimation was however the smallest when using tissue acceleration data, and is therefore the preferred way for characterizing wave propagation in the TD. Results showed that care should be taken when comparing the outcomes of cardiac SWE studies using a different wave characterization method and/or type of tissue motion in their data analysis.

Acknowledgements—The authors thank Vlaams Supercomputer Centrum for recourses provided for simulation computations. This work was supported by supported by the Research Foundation Flanders (FWO) grant GO92318N. Annette Caenen is supported by FWO grant 1211620N. Jan D'hooge has research collaboration with GE Vingmed.

Appendix A: Literature overview of different mechanical wave characterization methods reported in cardiac SWE

An overview of various analysis methods reported in literature for the cardiac SWE summarized in Table .

Table A.1 – Overview of reported analysis methods and resulting shear wave speed in healthy controls in cardiac SWE (this table does not give a comprehensive overview all cardiac SWE studies, but to summarizes studies that show differences in analysis approaches). In this table, MVC is classified as diastole and AVC as systole even though this is not necessarily true. The type of tissue motion is indicated with 'u' for displacements, 'v' for velocities and 'a' for accelerations (HV – healthy volunteer; IVS – interventricular septum; LV – left ventricle; LVFW - left ventricular free wall; PLAX – parasternal long-axis; AP4C – apical four chamber; PSAX – parasternal short-axis; MVC – mitral valve closure; AVC – aortic valve closure; ARF – acoustic radiation force).

	Subject	Region	View	Excitation type SWE	Analysed particle motion	Wave propagation characterization method	Reported end-metric	Result for healthy controls		Ref
								Diastole	Systole	
Animal	Canine (n=2)	LVFW	open chest	ARF	u	Time & frequency	speed	0.78 m/s	1.97 m/s	(Bouchard et al. 2011)
	Pigs (n=8)	LV	open chest	mechanical actuator	u	frequency	speed/shear modulus	2.01 m/s 1.81±0.80 kPa	4.63 m/s 21.14±7.72 kPa	(Urban et al. 2013)
	Pigs (n=22)	IVS	PLAX	MVC/AVC	v	Time	speed	0.8 – 3.2 m/s	1.4 – 6.3 m/s	(Vos et al. 2017)
	HV (n=5)	IVS	PLAX	AVC	v	frequency	shear modulus and viscosity	24 – 40 kPa 70-400 Pa·s		(Kanai 2005)
	Sheep (n=10)	LV	open chest; long axis	ARF	v	Time	speed/shear modulus	1.45 ± 0.32 m/s 2.17 ± 0.9 kPa	4.8 ± 1.4 m/s 24.9 ± 11 kPa	(Couade et al. 2011)
	Pigs (n=10)	LV	open chest	mechanical actuator	u	Time	shear modulus and viscosity	1.8 ± 0.7 kPa 2.5 ± 0.6 Pa·s	23 ± 7 kPa 5.0 ± 3.6 Pa·s	(Pislaru et al. 2014)
	Rat (n=6)	LV	isolated heart	ARF	v	Time	shear modulus	1.7 ± 0.8 kPa	8.6 ± 0.7 kPa	(Pernot et al. 2011)
Human	HV (n=26)	IVS	PLAX	MVC	a	Time	speed	4.04±0.96 m/s		(Cvijic et al. 2020)
	HV (n=10)	IVS	PLAX	AVC	v	Time	speed	3.6±0.4 m/s		(Strachinaru et al. 2020)
	HV (n=45)	IVS	PLAX	MVC/AVC	v	Time	speed	3.25 – 6.50 m/s	3.00 – 4.66 m/s	(Strachinaru et al. 2019)
	HV (n=10)	IVS	AP4C	AVC	a	Time	speed		5.41±1.25 m/s	(Brekke et al. 2014)
	HV (n=60)	IVS	PSAX	ARF	v	Time	shear modulus	4.47±1.68 kPa *(~2.03 m/s)*		(Villemain et al. 2019)

	HV (n=1)	IVS	PLAX	AVC	v	Time	speed		3.00 m/s	(Strachinaru et al. 2017b)
	HV (n=1)	LV	PLAX & AP4C	MVC/AVC	a	Time	speed		5.12±0.61 m/s	(Salles et al. 2019)

Appendix B: Describing the study population of the *in vivo* shear wave elastography measurements

This study describes in essence a methodology testing, so therefore the origin of the SWE data is irrelevant and consequently SWE measurements were randomly selected from the KU Leuven database to represent a wide range of SW speeds. The SWE data originated from the following three ongoing studies at the KU Leuven:

- healthy volunteers and patients that underwent a bicycle exercise stress test, with shear wave measurements at rest and during exercise (approved by the local ethical committee S60439).
- patients undergoing haemodialysis, with shear wave measurements taken before the start of haemodialysis (approved by the local ethical committee S62685).
- pigs with shear wave measurements at baseline, loading alterations (preload increase/decrease and afterload increase) and after the induction of an ischemia/reperfusion injury (approved by the Ethical Committee for Animal Experiments of KU Leuven P041/2019).

An overview of the structure of the *in vivo* shear wave data is presented in Table B.1.

Table B.1 – Structure of the study populations of the *in vivo* shear wave data used for analysis.

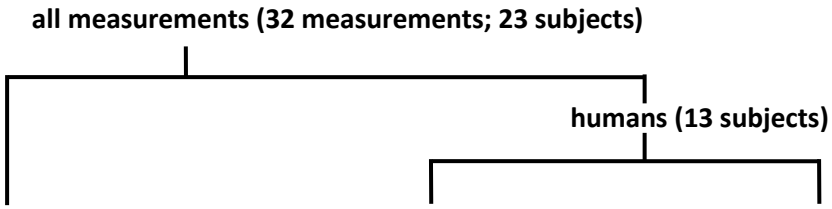

pigs (10 subjects)	
state	**measurements**
baseline	7
infarct	3
receiving dobutamine	3
afterload increase	2
preload decrease	2
preload increase	1

healthy volunteers (7 subjects)	
state	**measurements**
baseline	5
bicycle exercise	2

patients (6 subjects)	
state	**measurements**
baseline	6
bicycle exercise	1

References

Arnott PJ, Pfeiffer GW, Tavel ME. Spectral analysis of heart sounds: Relationships between some physical characteristics and frequency spectra of first and second heart sounds in normals and hypertensives. J Biomed Eng 1984;6:121–128. Available from: https://linkinghub.elsevier.com/retrieve/pii/0141542584900542

Bankman IN. Handbook of Medical Image Processing and Analysis. Elsevier, 2009.

Bernal M, Nenadic I, Urban MW, Greenleaf JF. Material property estimation for tubes and arteries using ultrasound radiation force and analysis of propagating modes. J Acoust Soc Am 2011;129:1344–1354. Available from: http://www.ncbi.nlm.nih.gov/pubmed/21428498

Bezy S, Duchenne J, Orlowska M, Amoni M, Caenen A, Keijzer L, Mccutcheon K, Ingelaere S, Cvijic M, Puvrez A, Vos H, D"hooge J, Voigt J. Natural shear wave propagation speed is influenced by both changes in myocardial structural properties as well as loading conditions. Eur Hear J - Cardiovasc Imaging 2021;22:167.

Bouchard RR, Hsu SJ, Palmeri ML, Rouze NC, Nightingale KR, Trahey GE. Acoustic Radiation Force-Driven Assessment of Myocardial Elasticity Using the Displacement Ratio Rate (DRR) Method. Ultrasound Med Biol 2011;37:1087–1100. Available from: https://linkinghub.elsevier.com/retrieve/pii/S030156291100202X

Brekke B, Nilsen LCL, Lund J, Torp H, Bjastad T, Amundsen BH, Stoylen A, Aase SA. Ultra-high Frame Rate Tissue Doppler Imaging. Ultrasound Med Biol 2014;40:222–231. Available from: https://linkinghub.elsevier.com/retrieve/pii/S030156291301020X

Caenen A, Pernot M, Shcherbakova DA, Mertens L, Kersemans M, Segers P, Swillens A. Investigating Shear Wave Physics in a Generic Pediatric Left Ventricular Model via In Vitro Experiments and Finite Element Simulations. IEEE Trans Ultrason Ferroelectr Freq Control 2017a;64:349–361. Available from: https://ieeexplore.ieee.org/document/7740062/

Caenen A, Thabit A, Pernot M, Shcherbakova D, Mertens L, Swillens A, Segers P. The effect of stretching on transmural shear wave anisotropy in cardiac shear wave elastography: An ex vivo and in silico study. IEEE Int Ultrason Symp IUS 2017b;.

Couade M, Pernot M, Messas E, Bel A, Ba M, Hagege A, Fink M, Tanter M. In Vivo quantitative mapping of myocardial stiffening and transmural anisotropy during the cardiac cycle. IEEE Trans Med Imaging 2011;30:295–305.

Cvijic M, Bézy S, Petrescu A, Santos P, Orlowska M, Chakraborty B, Duchenne J, Pedrosa J, Vanassche T, D'hooge J, Voigt J-U. Interplay of cardiac remodelling and myocardial stiffness in hypertensive heart disease: a shear wave imaging study using high-frame rate echocardiography. Eur Hear J - Cardiovasc Imaging 2020;21:664–672. Available from: https://academic.oup.com/ehjcimaging/article/21/6/664/5543492

E.M.Lifshitz LDL. Theory of Elasticity. Second Eng. Bristol: Pergamon Press, 1970.

Elgeti T, Knebel F, Hättasch R, Hamm B, Braun J, Sack I. Shear-wave Amplitudes Measured with Cardiac MR Elastography for Diagnosis of Diastolic Dysfunction. Radiology 2014;271:681–687. Available from: www.rsna.org/rsnarights.

Finel V. 3D ultrafast echocardiography: Toward a quantitative imaging of the myocardium. Université Sorbonne Paris Cité, 2018.

Golob M, Moss RL, Chesler NC. Cardiac Tissue Structure, Properties, and Performance: A Materials Science Perspective. Ann Biomed Eng 2014;42:2003–2013.

Guerra JA de AA, Trippia M, Pissaia A, Teixeira BC de A, Ivantes CAP. Acoustic radiation force impulse is equivalent to liver biopsy to evaluate liver fibrosis in patients with chronic hepatitis C and nonalcoholic fatty liver disease. Arq Gastroenterol 2015;52:234–238. Available from: http://www.scielo.br/scielo.php?script=sci_arttext&pid=S0004-28032015000300234&lng=en&tlng=en

Jayaraman J, Indiran V, Kannan K, Maduraimuthu P. Acoustic Radiation Force Impulse Imaging in Benign and Malignant Breast Lesions. Cureus 2017;9. Available from: http://www.cureus.com/articles/7354-acoustic-radiation-force-impulse-imaging-in-benign-and-malignant-breast-lesions

Kanai H. Propagation of spontaneously actuated pulsive vibration in human heart wall and in vivo viscoelasticity estimation. IEEE Trans Ultrason Ferroelectr Freq Control IEEE, 2005;52:1931–1942. Available from: http://ieeexplore.ieee.org/document/1561662/

Kanai H. Propagation of Vibration Caused by Electrical Excitation in the Normal Human Heart. Ultrasound Med Biol Elsevier Ltd, 2009;35:936–948. Available from: http://dx.doi.org/10.1016/j.ultrasmedbio.2008.12.013

Keijzer L, Bosch JG, Verweij MD, de Jong N, Vos HJ. Intra-Scan Variability of Natural Shear Wave Measurements. 2018 IEEE Int Ultrason Symp IEEE, 2018. pp. 1–4. Available from: https://ieeexplore.ieee.org/document/8580159/

Kijanka P, Urban MW. Phase Velocity Estimation With Expanded Bandwidth in Viscoelastic Phantoms and Tissues. IEEE Trans Med Imaging 2021;40:1352–1362.

Kou S, Caballero L, Dulgheru R, Voilliot D, De Sousa C, Kacharava G, Athanassopoulos GD, Barone D, Baroni M, Cardim N, Gomez De Diego JJ, Hagendorff A, Henri C, Hristova K, Lopez T, Magne J, De La Morena G, Popescu BA, Penicka M, Ozyigit T, Rodrigo Carbonero JD, Salustri A, Van De Veire N, Von Bardeleben RS, Vinereanu D, Voigt JU, Zamorano JL, Donal E, Lang RM, Badano LP, Lancellotti P. Echocardiographic reference ranges for normal cardiac chamber size: Results from the NORRE study. Eur Heart J Cardiovasc Imaging 2014;15:680–690.

Kvåle KF, Salles S, Lervik LCN, Støylen A, Løvstakken L, Samset E, Torp H. Detection of Tissue Fibrosis using Natural Mechanical Wave Velocity Estimation: Feasibility Study. Ultrasound Med Biol 2020;46:2481–2492. Available from: https://linkinghub.elsevier.com/retrieve/pii/S0301562920301940

Maksuti E, Widman E, Larsson D, Urban MW, Larsson M, Bjällmark A. Arterial Stiffness Estimation by Shear Wave Elastography: Validation in Phantoms with Mechanical Testing. Ultrasound Med Biol 2016;42:308–321.

Nagueh SF, Smiseth OA, Appleton CP, Byrd BF, Dokainish H, Edvardsen T, Flachskampf FA, Gillebert TC, Klein AL, Lancellotti P, Marino P, Oh JK, Popescu BA, Waggoner AD. Recommendations for the Evaluation of Left Ventricular Diastolic Function by Echocardiography: An Update from the American Society of Echocardiography and the European Association of Cardiovascular Imaging. J Am Soc Echocardiogr Elsevier Inc, 2016;29:277–314. Available from: http://dx.doi.org/10.1016/j.echo.2016.01.011

Nenadic IZ, Urban MW, Pislaru C, Escobar D, Vasconcelos L, Greenleaf JF. In vivo open- and closed-chest measurements of left-ventricular myocardial viscoelasticity using lamb wave dispersion ultrasound vibrometry (LDUV): a feasibility study. Biomed Phys Eng Express IOP Publishing, 2018;4:047001. Available from: https://iopscience.iop.org/article/10.1088/2057-1976/aabe41

Nightingale K, Rouze N, Rosenzweig S, Wang M, Abdelmalek M, Guy C, Palmeri M. Derivation and analysis of viscoelastic properties in human liver: Impact of frequency on fibrosis and steatosis staging. IEEE Trans Ultrason Ferroelectr Freq Control IEEE, 2015;62:165–175.

Pelivanov I, Gao L, Pitre J, Kirby MA, Song S, Li D, Shen TT, Wang RK, O'Donnell M. Does group velocity always reflect elastic modulus in shear wave elastography? J Biomed Opt 2019;24:1.

Pernot M, Couade M, Mateo P, Crozatier B, Fischmeister R, Tanter M. Real-Time Assessment of Myocardial Contractility Using Shear Wave Imaging. J Am Coll Cardiol Elsevier Inc., 2011;58:65–72. Available from: http://dx.doi.org/10.1016/j.jacc.2011.02.042

Pernot M, Couade M, Mateo P, Fischmeister R, Crozatier B, Tanter M. Dynamic and quantitative assessment of myocardial stiffness using shear wave imaging. 2010 7th IEEE Int Symp Biomed Imaging From Nano to Macro, ISBI 2010 - Proc 2010; Available from: http://www.mendeley.com/research/dynamic-quantitative-assessment-myocardial-stiffness-using-shear-wave-imaging

Petrescu A, Bézy S, Cvijic M, Santos P, Orlowska M, Duchenne J, Pedrosa J, Van Keer JM, Verbeken E, von Bardeleben S, Droogne W, Bogaert J, Van Cleemput J, D'hooge J, Voigt JU. Shear Wave Elastography Using High-Frame-Rate Imaging in the Follow-Up of Heart Transplantation Recipients. JACC Cardiovasc Imaging 2020;13:2304–2313. Available from: https://doi.org/10.1016/j.jcmg.2020.06.043

Petrescu A, Santos P, Orlowska M, Pedrosa J, Bézy S, Chakraborty B, Cvijic M, Dobrovie M, Delforge M, D'hooge J, Voigt JU. Velocities of Naturally Occurring Myocardial Shear Waves Increase With Age and in Cardiac Amyloidosis. JACC Cardiovasc Imaging 2019;12:2389–2398.

Pislaru C, Urban MW, Pislaru S V., Kinnick RR, Greenleaf JF. Viscoelastic Properties of Normal and Infarcted Myocardium Measured by a Multifrequency Shear Wave Method: Comparison with Pressure-Segment Length Method. Ultrasound Med Biol 2014;40:1785–1795. Available from: https://linkinghub.elsevier.com/retrieve/pii/S0301562914001525

Rose JL. Ultrasonic guided waves in solid media. New York: Cambridge University Press, 2014.

Rouze NC, Deng Y, Trutna CA, Palmeri ML, Nightingale KR. Characterization of Viscoelastic Materials Using Group Shear Wave Speeds. IEEE Trans Ultrason Ferroelectr Freq Control 2018;65:780–794. Available from: https://ieeexplore.ieee.org/document/8314723/

Salles S, Espeland T, Molares A, Aase SA, Hammer TA, Støylen A, Aakhus S, Lovstakken L, Torp H. 3D Myocardial Mechanical Wave Measurements: Toward In Vivo 3D Myocardial Elasticity Mapping. JACC Cardiovasc Imaging 2021;14:1495–1505.

Salles S, Lovstakken L, Aase SA, Bjastad TG, Torp H. Clutter Filter Wave Imaging. IEEE Trans Ultrason Ferroelectr Freq Control 2019;66:1444–1452. Available from: https://ieeexplore.ieee.org/document/8742662/

Santos P, Petrescu AM, Pedrosa JP, Orlowska M, Komini V, Voigt JU, D'Hooge J. Natural Shear Wave Imaging in the Human Heart: Normal Values, Feasibility, and Reproducibility. IEEE Trans Ultrason Ferroelectr Freq Control 2019;66:442–452.

Sarvazyan AP, Urban MW, Greenleaf JF. Acoustic Waves in Medical Imaging and Diagnostics. Ultrasound Med Biol 2013;39:1133–1146. Available from: https://linkinghub.elsevier.com/retrieve/pii/S0301562913000793

Savarese G, Lund LH. Global Public Health Burden of Heart Failure. Card Fail Rev 2017;03:7. Available from: https://www.cfrjournal.com/articles/global-public-health-burden-heart-failure

Strachinaru M, Bosch JG, Schinkel AFL, Michels M, Feyz L, de Jong N, Geleijnse ML, Vos HJ. Local myocardial stiffness variations identified by high frame rate shear wave echocardiography. Cardiovasc Ultrasound 2020;18:40. Available from: https://doi.org/10.1186/s12947-020-00222-1

Strachinaru M, Bosch JG, van Dalen BM, van Gils L, van der Steen AFW, de Jong N, Geleijnse ML, Vos HJ. Cardiac Shear Wave Elastography Using a Clinical Ultrasound System. Ultrasound Med Biol 2017a;43:1596–1606.

Strachinaru M, Bosch JG, van Dalen BM, van Gils L, van der Steen AFW, de Jong N, Geleijnse ML, Vos HJ. Cardiac Shear Wave Elastography Using a Clinical Ultrasound System. Ultrasound Med Biol 2017b;43:1596–1606.

Strachinaru M, Bosch JG, van Gils L, van Dalen BM, Schinkel AFL, van der Steen AFW, de Jong N, Michels M, Vos HJ, Geleijnse ML. Naturally Occurring Shear Waves in Healthy Volunteers and Hypertrophic Cardiomyopathy Patients. Ultrasound Med Biol 2019;45:1977–1986. Available from: https://linkinghub.elsevier.com/retrieve/pii/S0301562919301413

Treeby BE, Cox BT. k-Wave: MATLAB toolbox for the simulation and reconstruction of photoacoustic wave fields. J Biomed Opt

2010;15:021314.

Trutna CA, Rouze NC, Palmeri ML, Nightingale KR. Measurement of Viscoelastic Material Model Parameters Using Fractional Derivative Group Shear Wave Speeds in Simulation and Phantom Data. IEEE Trans Ultrason Ferroelectr Freq Control 2020;67:286–295. Available from: https://ieeexplore.ieee.org/document/8850040/

Urban MW, Pislaru C, Nenadic IZ, Kinnick RR, Greenleaf JF. Measurement of Viscoelastic Properties of In Vivo Swine Myocardium Using Lamb Wave Dispersion Ultrasound Vibrometry (LDUV). IEEE Trans Med Imaging 2013;32:247–261. Available from: http://ieeexplore.ieee.org/document/6323035/

Villemain O, Correia M, Mousseaux E, Baranger J, Zarka S, Podetti I, Soulat G, Damy T, Hagège A, Tanter M, Pernot M, Messas E. Myocardial Stiffness Evaluation Using Noninvasive Shear Wave Imaging in Healthy and Hypertrophic Cardiomyopathic Adults. JACC Cardiovasc Imaging 2019;12:1135–1145.

Voigt JU. Direct Stiffness Measurements by Echocardiography: Does the Search for the Holy Grail Come to an End? JACC Cardiovasc Imaging 2019;12:1146–1148.

Vos HJ, van Dalen BM, Heinonen I, Bosch JG, Sorop O, Duncker DJ, van der Steen AFW, de Jong N. Cardiac Shear Wave Velocity Detection in the Porcine Heart. Ultrasound Med Biol 2017;43:753–764. Available from: https://linkinghub.elsevier.com/retrieve/pii/S0301562916304124